Precise determination of the quadrupole transition matrix element of $^{40}Ca^{+}$ via branching-fraction and lifetime measurements

H. Shao,[1,2,3] Y. Huang,[1,2] H. Guan,[1,2,*] C. Li,[1,2] T. Shi,[1,2,4] and K. Gao[1,2,4,†]

[1]*State Key Laboratory of Magnetic Resonance and Atomic and Molecular Physics, Wuhan Institute of Physics and Mathematics, Chinese Academy of Sciences, Wuhan 430071, China*

[2]*Key Laboratory of Atomic Frequency Standards, Wuhan Institute of Physics and Mathematics, Chinese Academy of Sciences, Wuhan 430071, China*

[3]*University of Chinese Academy of Sciences, Beijing 100049, China*

[4]*Center for Cold Atom Physics, Chinese Academy of Sciences, Wuhan 430071, China*

(Received 16 September 2016; published 24 May 2017)

We report the experimental determination of the $4s\ ^2S_{1/2} \leftrightarrow 3d\ ^2D_{5/2}$ quadrupole transition matrix element in $^{40}Ca^{+}$ by measuring the branching fraction of the $3d\ ^2D_{5/2}$ state decaying into the ground state $4s\ ^2S_{1/2}$ and the lifetime of the $3d\ ^2D_{5/2}$ state, using a technique of a highly synchronized measurement sequence for laser control and highly efficient quantum state detection for quantum jumps. The measured branching fraction and improved lifetime are, respectively, 0.998(12) and 1.1649(44) s, which yield the value of the quadrupole transition matrix element (in absolute value) of 9.733(52) ea_0^2 with an uncertainty of 0.54%. The measured quadrupole transition matrix element is in good agreement with the most precise many-body atomic structure calculations. Our method can be universally applied to measurements of transition matrix elements in single ions and atoms of similar structure.

DOI: 10.1103/PhysRevA.95.053415

I. INTRODUCTION

Due to the environmental isolation and long interrogation time, a single trapped $^{40}Ca^{+}$ ion is an ideal system for an optical frequency standard [1], for quantum state engineering, and for atomic precision spectroscopy studies, such as the measurement of low-lying state lifetimes [2,3], branching fractions [4], and dipole transition matrix elements [5]. There are similar developments for $^{88}Sr^{+}$ [6,7] and $^{138}Ba^{+}$ [8,9]. Among many atomic properties, precise understanding of branching fractions and lifetimes is of particular importance to design optical frequency standards; this is because in many ion clocks, such as $^{40}Ca^{+}$, $^{88}Sr^{+}$, and $^{138}Ba^{+}$, the clock reference lines are dipole-forbidden quadrupole transitions. Thus a knowledge of lifetime and branching fraction is essential for characterizing relevant spectral lines. Also, in quantum information research, due to the long coherence time of the ground and metastable states, selected quadrupole transitions for encoding a quantum bit of information are used to realize quantum logic techniques [10,11]. In plasma physics, quadrupole transitions open an observational window into hot plasmas of low electron density [12]. In astrophysics, quadrupole transition lines provide information on structure and physical characteristics of interstellar clouds [13,14]. Since the existence of magic wavelengths for the $^{40}Ca^{+}$ clock transition has been demonstrated both in theory [15,16] and in experiment [17], all-optical trapped ion clocks are feasible to be realized in the foreseeable future. One important issue for building such a kind of trap is to overcome large ac Stark shifts due to the use of high optical power; thus it is necessary to take higher-order effects into account and the corresponding high-order transition matrix elements have to be considered [18]. Moreover, electric quadrupole transitions can be used to study atomic parity violation in heavy ions [19,20]. Finally, a strong motivation for the precise measurement of quadrupole transition matrix elements is to test many-body atomic theories [2,21–24].

In principle, dipole transition matrix elements in an atom or ion can be determined by considering ac Stark shifts when it is exposed to light, using the concept of magic wavelength, such as the work on ^{87}Rb [25] and on $^{40}Ca^{+}$ [17]. Dipole transition matrix elements can also be determined by comparing measurements of dispersive and absorptive light ion interactions [5]. However, for quadrupole transition matrix elements, there have been no experimental results for any alkali-metal-like ions, to our knowledge. On the other hand, there are only a few theoretical calculations [2,21–24] for the quadrupole transition matrix elements, where some of them are in disagreement. It is therefore desirable to resolve this situation experimentally. In this paper, we propose a method to precisely determine the quadrupole transition matrix element by measuring relevant branching fraction and lifetime. Our method is very suitable for a state with the natural lifetime on the order of seconds. We demonstrate our approach for the case of the $^{40}Ca^{+}$ ion. More specifically, by accurately controlling experimental conditions, such as ion collision with background gases, laser purity, linewidth and stability, magnetic shift and noise, ion heating and loss effects, shelving and pumping rates, state detection errors, and the number of measurements, together with the improved method [9] for $^{138}Ba^{+}$, we report a determination of the quadrupole transition matrix moment (in absolute value) in $^{40}Ca^{+}$ involving the metastable $3d\ ^2D_{5/2}$ state and the ground $4s\ ^2S_{1/2}$ state by measuring the $3d\ ^2D_{5/2}$ state lifetime and the branching fraction of $3d\ ^2D_{5/2}$ decaying into $4s\ ^2S_{1/2}$, based on the relationship [26] among the branching fraction Γ_{ki}, the lifetime τ_k, and the transition rate A_{ki}, i.e., $\Gamma_{ki} = \tau_k A_{ki}$, where index k is for the upper $3d\ ^2D_{5/2}$ state and i is for the lower $4s\ ^2S_{1/2}$ state. The transition rate

*guanhua@wipm.ac.cn
†klgao@wipm.ac.cn

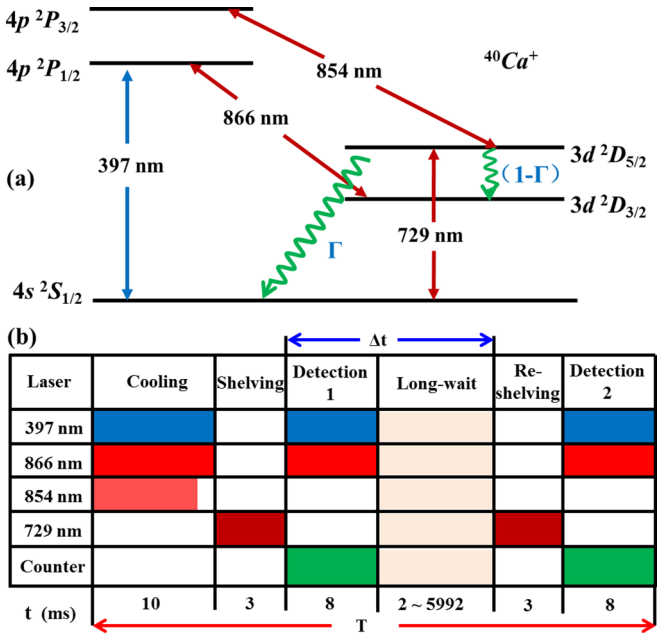

FIG. 1. (a) Partial energy-level diagram of $^{40}Ca^{+}$. The 397- and 866-nm lasers are for cooling and detection, the 854-nm laser is for quenching, and the 729-nm laser is for shelving. (b) A simplified measurement sequence.

is further related to the quadrupole transition matrix moment $\langle k\|E2\|i\rangle$ by $A_{ki} = \frac{1.11995\times10^{18}}{\lambda^5 g_k}|\langle k\|E2\|i\rangle|^2$, where g_k= 6 and λ is the transition wavelength in Å [1]. Our method can in principle be applied to other systems such as Ba^{+}, Sr^{+}, Ra^{+}, Ac^{2+}, and Th^{3+} with a similar structure.

II. EXPERIMENTAL PROCEDURE

The $^{40}Ca^{+}$ ion is first trapped and laser cooled in a miniature ring Paul trap. A high-efficiency quantum state detection method for fluorescence counting and a highly synchronized measurement sequence for laser control are adopted. Figure 1(a) shows the relevant energy levels and transition lines. Once the ion is shelved to the $3d\,^2D_{5/2}$ state, it can spontaneously decay into the $4s\,^2S_{1/2}$ ground state with the branching fraction Γ and to the $3d\,^2D_{3/2}$ state with the branching fraction $1-\Gamma$ [9] during a long-wait time Δt. The probability $P_{5/2}$ that the ion remains in the excited state after a time Δt obeys the exponential law $P_{5/2} = e^{-\Delta t/\tau_{5/2}}$, where $\tau_{5/2}$ is the $3d\,^2D_{5/2}$ state lifetime. Figure 1(b) shows a simplified sequence for the lifetime and branching-fraction measurements. The branching-fraction sequence consists of five steps: cooling, shelving, long-wait Δt for decay, reshelving, and state detection. In the first step, both the 397- and 866-nm lasers are turned on for 10 ms to cool the ion to the Lamb-Dicke regime in each cycle, and the 854-nm laser is then applied for the first 8 ms to pump the ion to $4p\,^2P_{3/2}$, followed by a fast decay to the $4s\,^2S_{1/2}$ ground state. In the second step, the 729-nm laser is applied for 3 ms to shelve the ion to the $3d\,^2D_{5/2}$ state, followed by an 8-ms pulse for state detection. When the ion is successfully shelved, the fluorescence at 397 nm decreases to the background level, which indicates a valid measurement; otherwise the next cycle starts. Then a long-wait period Δt is performed, during which the ion decays spontaneously with no laser light disturbing the process. In the fourth step, after a long-wait time Δt for decay, the 729-nm laser is applied for 3 ms so that the ion decaying into $4s\,^2S_{1/2}$ can be reshelved. Finally, the quantum state detection is performed and the process is to observe the fluorescence signal of the ions by turning the 397- and 866-nm lasers on. We need to note that all time intervals and laser's powers described above are chosen by many corresponding independent measurements. For those ions always staying in $3d\,^2D_{5/2}$, or decaying into $4s\,^2S_{1/2}$ first followed by a reshelving to $3d\,^2D_{5/2}$, the fluorescence signal shows "dark"; otherwise it appears "bright". The final probability $P_{\rm dark}$ that the ion is in the $3d\,^2D_{5/2}$ state at the end of the procedure depends on the probability $P_{5/2}$ of the spontaneous decay from $3d\,^2D_{5/2}$ during the wait time, the branching fraction Γ from $3d\,^2D_{5/2}$ to $4s\,^2S_{1/2}$, the reshelving efficiency $P_{\rm resh}$ by the 729-nm laser, and the probability $1-P_{3/2}$ for the decay from $3d\,^2D_{3/2}$ to $4s\,^2S_{1/2}$ during the wait time. Finally, the probability that the ion will be found in the dark state can be determined from the following three procedures. The first one is the probability $P_{5/2}$ of the ion always staying in $3d\,^2D_{5/2}$ during a certain delay time Δt. The second one is the probability $(1-P_{5/2})\Gamma P_{\rm resh}$ of the ion decaying into $4s\,^2S_{1/2}$ while reshelved to $3d\,^2D_{5/2}$ by a 729-nm laser. The third one is the probability $(1-P_{5/2})(1-\Gamma)(1-P_{3/2})P_{\rm resh}$ of the ion decaying into $3d\,^2D_{3/2}$ and then into $4s\,^2S_{1/2}$ and finally being reshelved to $3d\,^2D_{5/2}$. But if the ion always stays in $3d\,^2D_{5/2}$ and does not decay into other states, when acted upon by the reshelving 729-nm laser, it can induce a stimulated radiation to $4s\,^2S_{1/2}$ with the probability $P_{\rm SR}$. We can thus establish the following equation:

$$P_{\rm dark} = P_{5/2}(1-P_{\rm SR}) + (1-P_{5/2})\Gamma P_{\rm resh} + (1-P_{5/2})(1-\Gamma)(1-P_{3/2})P_{\rm resh}. \quad (1)$$

Solving for Γ yields

$$\Gamma = \frac{P_{\rm dark} - P_{5/2}(1-P_{\rm SR}) - (1-P_{5/2})(1-P_{3/2})P_{\rm resh}}{(1-P_{5/2})P_{3/2}P_{\rm resh}}. \quad (2)$$

In order to extract the branching fraction Γ from the experimental data, we need to measure independently the probabilities $P_{5/2}$, $P_{3/2}$, $P_{\rm dark}$, $P_{\rm SR}$, and $P_{\rm resh}$ at a certain wait time Δt. Here, we chose Δt=100 ms. In the experiment, the reshelving probability related to the branching fraction is easily affected by the 729-nm laser frequency shift and by magnetic-field perturbation. In order to maintain a stable reshelving probability, we need to minimize the magnetic field at the position of the ion by using the Hanle effect. The final ten Zeeman spectral lines are measured with full width of about 500 Hz. Also, a Ti:sapphire laser (Coherent Inc, MBR110) at 729 nm is locked to a high-finesse ULE (ultra-low-expansion) cavity using the Pound-Drever-Hall scheme, with the typical linewidth (full width at half maximum) of the laser being ~1 Hz [27]. The cooling and detection lasers at 397 and 866 nm are frequency stabilized to the ultranarrow linewidth 729-nm laser by a transfer cavity [28]. To reduce the residual lights that affect our measurements, all lights are controlled by acousto-optic modulators and mechanical shutters synchronously.

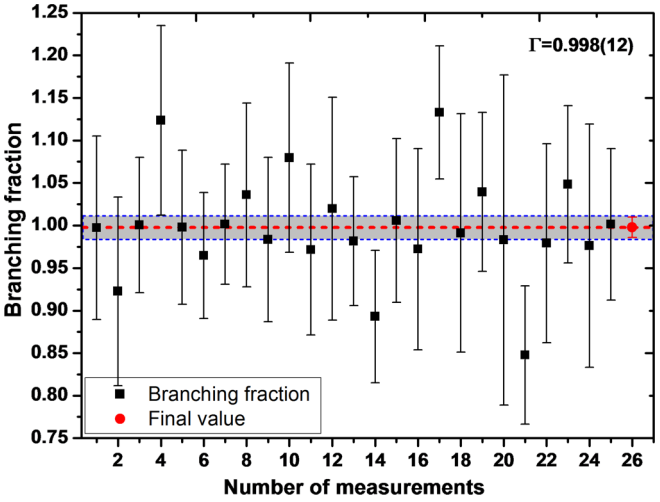

FIG. 2. Measured data points for the branching-fraction measurements for decay from $3d\,^2D_{5/2}$ into $4s\,^2S_{1/2}$. The final value is determined using 1.5×10^6 measurement cycles.

After having repeated 1.5×10^6 effective cycles of measurements, to begin with, the individual probabilities $P_{5/2} = 0.91781(34)$ and $P_{3/2} = 0.91979(45)$ are obtained. Although the 729-nm laser applied is power stabilized and optical fiber noise is canceled, the probabilities P_{dark}, P_{SR}, and P_{resh} are still found to be slightly varied with laser power fluctuation and beam pointing direction, and it is difficult to make a high accuracy measurement by averaging. An effective way is to calculate the branching fraction using those measured probabilities in some suitable cycles, then continuously repeat this process by a large number of measurements, which can not only maintain a stable environment for measurement within a short time but also obtain the probabilities with high precision. Finally, after 1.5×10^6 cycles of measurements, the $3d\,^2D_{5/2}$ to $4s\,^2S_{1/2}$ branching fraction is obtained as $\Gamma = 0.998(12)$. The measured results are shown in Fig. 2.

For the lifetime measurement of the $3d\,^2D_{5/2}$ state, the sequence is similar to the measurement of the branching fraction but without including the reshelving pulse. After cooling and shelving, we need to confirm whether the ion is shelved to $3d\,^2D_{5/2}$. Only in the first state detection period where the fluorescence shows a background level is the measurement regarded as valid. After a long-wait time Δt for decay, the second state detection is performed to detect whether the ion still stays in $3d\,^2D_{5/2}$ or has decayed into $4s\,^2S_{1/2}$. If not, the fluorescence remains at the background level. In this experiment, for each wait time Δt, the measurement is repeated more than 30 000 times and Δt is set to vary from 10 to 6000 ms. The spontaneous decay probability P changes with Δt and is defined as the ratio of two quantum jump numbers that are counted, respectively, in the second and the first detections. The $3d\,^2D_{5/2}$ state lifetime is then determined from the exponential law $P = e^{-\Delta t/\tau_{5/2}}$. Using the measured data points shown in Fig. 3(a) and the method of linear regression and least-squares fitting, we obtain the natural lifetime $\tau_{5/2} = 1.1650(43)$ s with 95% confidence. Also, the detected mean time when the ion stays in the $3d\,^2D_{5/2}$ state during Δt is determined from the law $t_i = \Delta t e^{-\Delta t/\tau_{5/2}}$.

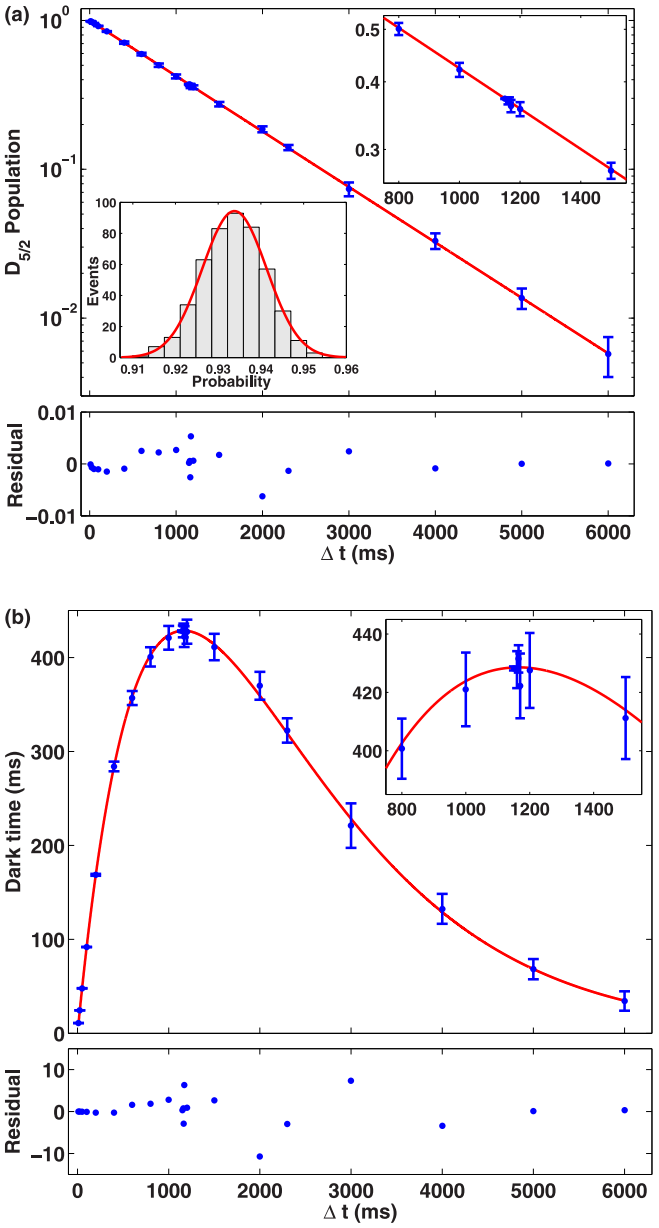

FIG. 3. Two fitting methods to the data points for the $3d\,^2D_{5/2}$ state lifetime measurement in $^{40}Ca^+$. (a) The fitting curve determined by the method of linear regression and least-squares fit yields the lifetime $\tau_{5/2} = 1.1650(43)$ s with 95% confidence (2σ). The lower left quarter shows the verified result of the normal distribution. (b) The fitting curve determined by the maximum likelihood fit yields the lifetime $\tau_{5/2} = 1.1649(34)$ s with 95% confidence. Each point represents 30 000 measurements per Δt from 10 to 6000 ms. The lower diagram shows the residuals between the data points and the fitting curve.

Using the measured data points shown in Fig. 3(b) and the method of maximum likelihood fit [6,29] yields the lifetime $\tau_{5/2} = 1.1649(34)$ s with 95% confidence. This confidence interval is 2σ standard uncertainty in the two estimates of $\tau_{5/2}$. The final mean fitting value is 1.1650(43) s by the two independent methods. For each probability at different Δt, we carried out large numbers of measurements to reduce statistical uncertainty. Since the spontaneous decay probability

obeys a normal distribution, the statistical uncertainty can be effectively reduced by averaging. The normal distribution is verified by measuring the spontaneous decay probability from $3d\,^2D_{5/2}$ state to $4s\,^2S_{1/2}$ state at $\Delta t = 80$ ms, as shown in the lower left quarter of Fig. 3(a). Each event represents the number of quantum jumps during 1200 experimental cycles, and 480 of such events (480×1200 measurement cycles in total) are conducted to study the probability distribution. The result shows that the probability of spontaneous decay obeys a normal distribution $f(p) = \frac{1}{\sqrt{2\pi}\sigma}\exp(-\frac{(p-\mu)^2}{2\sigma^2})$, the mean number is $\mu = 0.93377$, and the standard uncertainty is $\sigma = 0.0076$. Moreover, we also used a statistical tool like the chi-squared test to check that the results really do represent the normal distribution.

III. EVALUATION OF UNCERTAINTIES

The branching-fraction and lifetime measurements are affected by many factors, such as collision, ion heating, impure composition, laser coupling, and pumping rate. The final branching fraction obtained has been corrected by these factors. These physical effects can also affect the observed lifetime according to the formula [30] $1/\tau_m = 1/\tau_{\rm nat} + \sum_i \gamma_i$, where τ_m and $\tau_{\rm nat}$ are, respectively, the measured and natural lifetimes, and γ_i represent contributions from other effects. In our experiment, the 397- and 866-nm lasers for the cooling cycle are commercial semiconductor diode lasers, which may contain other spectral components that can induce unwanted excitations. Compared to our previous work [2], three improvements are made to reduce the influence on the measured lifetime. The first improvement is the use of a 406-nm narrow-band optical filter that was inserted in the 397-nm beam path to filter the 393-nm spectrum component contained in the 397-nm laser's spectrum. For this filter, the 393-nm laser's transmittance is less than 0.46%, after which the residual component (the 397-nm power is about 10.2 μW, which corresponds to the intensity of the 393-nm component far below 0.047 μW after passing the filter) is unable to excite the dipole excitation transition of $4s\,^2S_{1/2} \rightarrow 4p\,^2P_{3/2}$. The second improvement is the use of two 866-nm narrow-band optical filters in the 866-nm beam to filter out the 854-nm component. With these two filters, the 866-nm laser's transmittance is about 81% while the 854-nm laser's transmittance is less than 0.027%; so the residual component (the power of the 866-nm laser is about 450 μW, which corresponds to the power of the 854-nm component far below 0.12 μW after passing the filter) cannot induce the transition from $3d\,^2D_{5/2}$ to $4p\,^2P_{3/2}$ during the detection time. The third improvement is an increase of the sample size from 5000 to 30 000 for each delay time Δt, which greatly reduces the statistical error.

Furthermore, the main errors affecting the measured lifetime are analyzed. The first one is the collision of the ion with the rare background gases in the ultra-high-vacuum chamber. This process depopulates the $3d\,^2D_{5/2}$ state and results in a two-state mixing [30], which shortens the measured metastable lifetime. The collision rate can be monitored by recording the number of quantum jumps during the absence of the 729- and 854-nm lasers. With less than 1.0×10^{-8} Pa background pressure, about 0.022(14) quantum jumps are observed per minute at different times where each procedure lasts 60 min and is repeated nine times, resulting in a maximum collision rate of $0.37(23) \times 10^{-6}$/ms. The corresponding contribution to the $3d\,^2D_{5/2}$ state lifetime is $\delta\tau_{5/2} = 0.5(3)$ ms. The heating of the ion trap also affects the measured lifetime, but through the rf-photon correlation method [31] and selecting a suitable parameter the excess micromotion of the ion can be minimized. Another factor is that of the laser powers applied, but bringing in narrow-band optical filters in 397- and 866-nm routes as described above has filtered most of the unwanted components. The pumping rate also affects the measured lifetime and branching fraction. If the 854-nm laser does not pump the ion from $3d\,^2D_{5/2}$ to $4p\,^2P_{3/2}$, the rate for this spontaneous transition is 0.0014(5), which changes the measured lifetime by $\delta\tau_{5/2} = -1.6(6)$ ms [21]. The wrong state detection counting, due to Poisson noise in the photomultiplier tube and the spontaneous decay during the detection period, can be overcome by properly choosing a threshold value to discriminate the fluorescence of the ion in $4s\,^2S_{1/2}$ and $3d\,^2D_{5/2}$. The state detection error caused by the noise is 10^{-6} [32], which is negligible, whereas the error caused by the spontaneous decay is $0.8(7) \times 10^{-3}$, which changes the measured $3d\,^2D_{5/2}$ state lifetime by $\delta\tau_{5/2} = 1.0(8)$ ms. All factors affecting the measurements of the $3d\,^2D_{5/2}$ lifetime are summarized in Table I. The final result for the $3d\,^2D_{5/2}$ lifetime, after correction, is $\tau_{5/2} = 1.1649(44)$ s. Our result has improved the recently measured result of [2] by a factor of 2.

TABLE I. Error evaluation for the measurement of the lifetime of the $3d\,^2D_{5/2}$ state. The detailed analysis is described in the text. The systematic errors consist of errors due to the laser's intensities, collision with background gases, heating, etc. The statistical error refers to the error in the data analysis.

Effect	Shift (ms)	Uncertainty (ms)
Collision depopulation	0.5	0.3
Heating and ion loss		<0.1
397-nm laser power		<0.1
866-nm laser power		<0.1
854-nm pumping rate	−1.6	0.6
Photon counting	1.0	0.8
Statistical		4.3
Total error	−0.1	4.4

IV. CONCLUSIONS

With our measured branching fraction and lifetime, we can now extract the experimental values of the $4s\,^2S_{1/2} \leftrightarrow 3d\,^2D_{5/2}$ quadrupole transition rate and transition matrix element (in absolute value), which are, respectively, 0.8567(108) s^{-1} and 9.733(52) ea_0^2 at the levels of 1.08 and 0.54%. A comparison of recently measured and calculated quadrupole transition matrix elements is shown in Fig. 4. Those calculations are a delicate and sophisticated task, in which the relativistic many-body perturbation theory method and coupled-cluster method are adopted, and Breit interaction and vacuum polarization effect are taken into account. Our result is in good agreement with

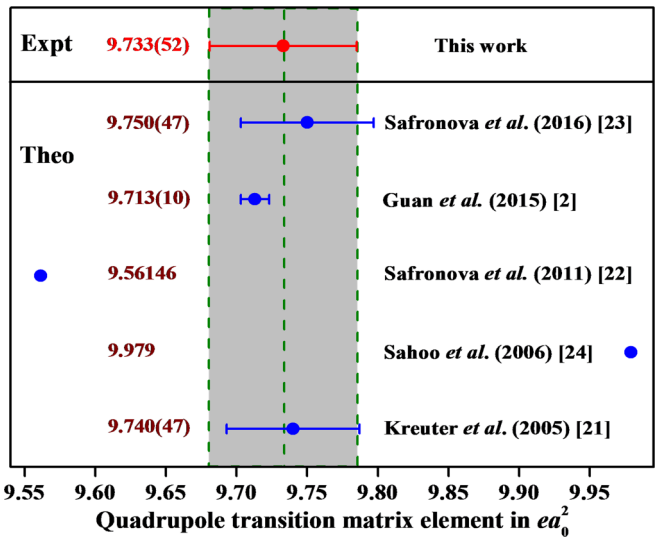

FIG. 4. Comparison of recently measured and calculated quadrupole transition matrix elements.

the theoretical values of 9.740(47) ea_0^2 and 9.750(47) ea_0^2 by M. S. Safronova and coworkers in Refs. [21,23] and 9.713(10) ea_0^2 by Guan *et al.* in Ref. [2].

In summary, with the development of a single-ion manipulation technique and laser spectroscopy methods, we have measured the $3d\ ^2D_{5/2}$ state lifetime in $^{40}Ca^+$, which is $\tau_{5/2} = 1.1649(44)$ s, with the uncertainty of 0.38%, a factor of 2 improvement over the previous measurement. Meanwhile, we have measured the branching fraction for the decay $3d\ ^2D_{5/2} \rightarrow 4s\ ^2S_{1/2}$ as 0.998(12). With these two measured results, we have extracted the experimental value of the $4s\ ^2S_{1/2} \leftrightarrow 3d\ ^2D_{5/2}$ quadrupole transition matrix element 9.733(52) ea_0^2, at the level of 0.54%. Our results can serve as a test bed for atomic structure calculations and for high-precision laser spectroscopy [33]. Nevertheless, the main sources of uncertainties originate from the statistical errors in the lifetime measurement, collision with background gases, and the existence of multiple decay channels in the branching-fraction measurement. Further improvement in accuracy is still possible by collecting a larger number of quantum jumps under a better vacuum condition.

ACKNOWLEDGMENTS

We thank Z.-C. Yan, P. Dubé, A. Derevianko, and B. K. Sahoo for fruitful discussion. This work was financially supported by the Strategic Priority Research Program of the Chinese Academy of Sciences (Grant No. XDB21030100), the National Natural Science Foundation of China (Grants No. 91336211, No. 11634013, No. 11474318, and No. 11622434), and by Chinese Academy of Sciences.

[1] Y. Huang, H. Guan, P. Liu, W. Bian, L. Ma, K. Liang, T. Li, and K. Gao, Phys. Rev. Lett. **116**, 013001 (2016).
[2] H. Guan, H. Shao, Y. Qian, Y. Huang, P.-L. Liu, W. Bian, C.-B. Li, B. K. Sahoo, and K.-L. Gao, Phys. Rev. A **91**, 022511 (2015).
[3] H. Shao, Y. Huang, H. Guan, Y. Qian, and K. Gao, Phys. Rev. A **94**, 042507 (2016).
[4] M. Ramm, T. Pruttivarasin, M. Kokish, I. Talukdar, and H. Häffner, Phys. Rev. Lett. **111**, 023004 (2013).
[5] M. Hettrich, T. Ruster, H. Kaufmann, C. F. Roos, C. T. Schmiegelow, F. Schmidt-Kaler, and U. G. Poschinger, Phys. Rev. Lett. **115**, 143003 (2015).
[6] V. Letchumanan, M. A. Wilson, P. Gill, and A. G. Sinclair, Phys. Rev. A **72**, 012509 (2005).
[7] J.-P. Likforman, V. Tugayé, S. Guibal, and L. Guidoni, Phys. Rev. A **93**, 052507 (2016).
[8] J. Gurell, E. Biémont, K. Blagoev, V. Fivet, P. Lundin, S. Mannervik, L.-O. Norlin, P. Quinet, D. Rostohar, P. Royen, and P. Schef, Phys. Rev. A **75**, 052506 (2007).
[9] C. Auchter, T. W. Noel, M. R. Hoffman, S. R. Williams, and B. B. Blinov, Phys. Rev. A **90**, 060501(R) (2014).
[10] C. F. Roos, M. Chwalla, K. Kim, M. Riebe, and R. Blatt, Nature (London) **443**, 316 (2006).
[11] J. Benhelm, G. Kirchmair, C. F. Roos, and R. Blatt, Nat. Phys. **4**, 463 (2008).
[12] H. P. Summers, N. R. Badnell, M. G. O'Mullane, A. D. Whiteford, R. Bingham, B. J. Kellett, J. Lang, K. H. Behringer, U. Fantz, K. D. Zastrow, S. D. Loch, M. S. Pindzola, D. C. Griffin, and C. P. Ballance, Plasma Phys. Contr. F. **44**, B323 (2002).
[13] D. E. Welty, D. C. Morton, and L. M. Hobbs, Astrophys. J. Suppl. **106**, 533 (1996).
[14] J. Kwan and W. Fischer, Mon. Not. R. Astron. Soc. **411**, 2383 (2011).
[15] Y.-B. Tang, H.-X. Qiao, T.-Y. Shi, and J. Mitroy, Phys. Rev. A **87**, 042517 (2013).
[16] J. Kaur, S. Singh, B. Arora, and B. K. Sahoo, Phys. Rev. A **92**, 031402(R) (2015).
[17] P.-L. Liu, Y. Huang, W. Bian, H. Shao, H. Guan, Y.-B. Tang, C.-B. Li, J. Mitroy, and K.-L. Gao, Phys. Rev. Lett. **114**, 223001 (2015).
[18] V. D. Ovsiannikov, S. I. Marmo, V. G. Palchikov, and H. Katori, Phys. Rev. A **93**, 043420 (2016).
[19] B. K. Sahoo, R. Chaudhuri, B. P. Das, and D. Mukherjee, Phys. Rev. Lett. **96**, 163003 (2006).
[20] B. K. Sahoo, T. Aoki, B. P. Das, and Y. Sakemi, Phys. Rev. A **93**, 032520 (2016).
[21] A. Kreuter, C. Becher, G. P. T. Lancaster, A. B. Mundt, C. Russo, H. Häffner, C. Roos, W. Hänsel, F. Schmidt-Kaler, R. Blatt, and M. S. Safronova, Phys. Rev. A **71**, 032504 (2005).
[22] U. I. Safronova and M. S. Safronova, Can. J. Phys. **89**, 465 (2011).
[23] U. I. Safronova, M. S. Safronova, and W. R. Johnson, Phys. Rev. A **95**, 042507 (2017).
[24] B. K. Sahoo, Md. R. Islam, B. P. Das, R. K. Chaudhuri, and D. Mukherjee, Phys. Rev. A **74**, 062504 (2006).
[25] C. D. Herold, V. D. Vaidya, X. Li, S. L. Rolston, J. V. Porto, and M. S. Safronova, Phys. Rev. Lett. **109**, 243003 (2012).
[26] D. K. Nandy, Y. Singh, B. K. Sahoo, and C. Li, J. Phys. B **44**, 225701 (2011).

[27] W. Bian, Y. Huang, H. Guan, P. Liu, L. Ma, and K. Gao, Rev. Sci. Instrum. **87**, 063121 (2016).
[28] W. Qu, Y. Huang, H. Guan, X. Huang, and K. Gao, Chin. J. Lasers **38**, 0802008 (2011).
[29] Y. Pawitan, *In All Likelihood: Statistical Modelling and Inference Using Likelihood* (Oxford University, Oxford, 2001).
[30] P. A. Barton, C. J. S. Donald, D. M. Lucas, D. A. Stevens, A. M. Steane, and D. N. Stacey, Phys. Rev. A **62**, 032503 (2000).
[31] D. J. Berkeland, J. D. Miller, J. C. Bergquist, W. M. Itano, and D. J. Wineland, J. Appl. Phys. **83**, 5025 (1998).
[32] C. Roos, Ph.D. thesis, University of Innsbruck, 2000.
[33] M. Chwalla, J. Benhelm, K. Kim, G. Kirchmair, T. Monz, M. Riebe, P. Schindler, A. S. Villar, W. Hänsel, C. F. Roos, R. Blatt, M. Abgrall, G. Santarelli, G. D. Rovera, and P. Laurent, Phys. Rev. Lett. **102**, 023002 (2009).